INTERNATIONAL JOURNAL FOR NUMERICAL METHODS IN FLUIDS, VOL. 19, 795–813 (1994)

# AN ELEMENT LEVEL ZERO-DIVERGENCE FINITE ELEMENT APPROACH

A. N. F. MACK*

*School of Mechanical Engineering, University of Technology, Sydney, PO Box 123, Broadway, NSW 2007, Australia*

## SUMMARY

An innovative idea for the solution of viscous incompressible flows, in which the equation for conservation of mass is satisfied at the element level, is termed the solenoidal finite element approach. The term 'solenoidal' derives from the fact that the velocity components need to be solenoidal, i.e. to have zero divergence. The difficulty with this idea centres on the construction of a specialized element in which the velocity components are constrained to be solenoidal by the nature of their interpolation functions. If such an element can be constructed, then the pressure is suppressed from the prime solution. This has obvious attractions, although recourse to another novel idea is needed for its eventual retrieval. The validity of these ideas is demonstrated herein by the results for some classical benchmark problems. Where possible, comparisons are made with other results, both from other codes and from the literature.

KEY WORDS Viscous Incompressible Solenoidal Finite element Square cavity Backward step

## INTRODUCTION

In connection with finite element solutions to viscous incompressible flows, an idea which has received scant attention is the solenoidal approach. The attraction of this approach is the inherent satisfaction of the continuity constraint and the uncoupling of the pressure from the prime solution. Early reviews[1,2] of finite element solution methods commented on the difficulty, if not impossibility, of this approach. The author, nevertheless, was attracted by the novelty of the idea and, after considerable effort, had success.[3–5] In the process it was demonstrated how the three main primitive variable approaches (solenoidal, penalty function, Lagrange multiplier) are just different manifestations of the imposition of the continuity constraint.[4,5]

Another approach which appears to possess the same attraction as the solenoidal approach centres on the introduction of the streamfunction. The drawback with this approach is a restriction on the spatial dimensions and a problem with the specification of the resulting boundary conditions.

The difficulty with the solenoidal approach centres on the construction of an admissible element, one which exhibits zero divergence. To date, such elements have proved somewhat elusive. Several elements[6–8] which purport to be solenoidal are in fact not inherently solenoidal, i.e. do not exhibit zero divergence as entities by themselves. These elements tend to have discontinuous pressure and thus the equations associated with the continuity constraint for each element are independent of the remainder of the elements, so that these equations can be condensed into the interpolation functions for the velocity components. Another example[9]

* Part of the research for this paper was undertaken whilst the author was on leave at the Institute for Computational Fluid Dynamics, University of Oxford, Oxford, U.K.

CCC 0271–2091/94/210795–19

*Received November 1993*
*Revised April 1994*

achieves the desired effect only in conjunction with neighbouring elements. The element which is discussed in this paper, on the other hand, is a development of the first genuine solenoidal element.[3,4,10]

Also, this paper presents, for the first time for the solenoidal approach, a viable means for the retrieval of the pressure.

## INTEGRAL FORMULATION

Consider the steady plane laminar flow of an incompressible Newtonian fluid whose viscosity is constant. The governing equations for this case take the form

$$u_x + v_y = 0, \tag{1}$$

$$\frac{1}{Re}\nabla^2 u - p_x = uu_x + vu_y, \tag{2a}$$

$$\frac{1}{Re}\nabla^2 v - p_y = uv_x + vv_y, \tag{2b}$$

where $p$ is the pressure with respect to some datum, $u$ is the velocity component in the $x$-direction and $v$ is the velocity component in the $y$-direction, all of which have been normalized, in doing so introducing the Reynolds number $Re$.

The finite element method operates, not on the differential equations, but on an integral formulation. Such a formulation can be obtained from an inner product with the arbitrary variations $\delta p$, $\delta u$ and $\delta v$ so that

$$\int_A \delta p(u_x + v_y)\,\mathrm{d}A + \int_A \delta u\left(\frac{1}{Re}\nabla^2 u - p_x - uu_x - vu_y\right)\mathrm{d}A + \int_A \delta v\left(\frac{1}{Re}\nabla^2 v - p_y - uv_x - vv_y\right)\mathrm{d}A = 0, \tag{3}$$

where $A$ is the integration domain. With the utilization of Green's theorem this becomes

$$\frac{1}{Re}\int_A (\delta u_x u_x + \delta v_x v_x + \delta u_y u_y + \delta v_y v_y)\,\mathrm{d}A + \int_A [\delta u(uu_x + vu_y) + \delta v(uv_x + vv_y)]\,\mathrm{d}A = \int_A [\delta(u_x + v_y)p + \delta p(u_x + v_y)]\,\mathrm{d}A + \int_s \left[\delta u\left(\frac{1}{Re}u_n - \alpha p\right) + \delta v\left(\frac{1}{Re}v_n - \beta p\right)\right]\mathrm{d}s, \tag{4}$$

where $\alpha$ and $\beta$ are the direction cosines for the normal $n$ to the boundary $s$.

Although often not formulated as such, the main primitive variable approaches all follow this path. However, the solenoidal approach then takes the radical step which recognizes the advantage to be gained from the imposition at the element level of velocity components with zero divergence. If this can be achieved, then

$$\frac{1}{Re}\int_A (\delta u_x u_x + \delta v_x v_x + \delta u_y u_y + \delta v_y v_y)\,\mathrm{d}A + \int_A [\delta u(uu_x + vu_y) + \delta v(uv_x + vv_y)]\,\mathrm{d}A = \int_s \left[\delta u\left(\frac{1}{Re}u_n - \alpha p\right) + \delta v\left(\frac{1}{Re}v_n - \beta p\right)\right]\mathrm{d}s, \tag{5}$$

whereupon the pressure is eliminated from the prime solution. Note, however, that equation (5) is dependent on the satisfaction, not of the solenoidal constraint (1), but of the weaker statement

$$\delta \int_A p(u_x + v_y)\, \mathrm{d}A = 0. \tag{6}$$

## SOLENOIDAL ELEMENT

As already mentioned, the difficulty with the solenoidal approach centres on the construction of an element for the velocity components. A triangular element is chosen, in part, to facilitate isotropic polynomial expansions. Complete quartic expansions, each of 15 terms, are selected to provide a number of degrees of freedom in excess of that needed to be conforming with which to impose the desired constraint. Although equation (5) indicates that a Lagrange element is permissible, higher-order nodal parameters are included to reduce the problem dimensions and hence the storage requirements.

As it happens, it is not possible to construct a conforming element which is pointwise solenoidal, i.e. one which satisfies equation (1) at all points in the element. A compromise, then, is to impose the constraint on the average over the element such that

$$\int_{A_e} (u_x + v_y)\, \mathrm{d}A = 0. \tag{7}$$

This is achieved through the use of the Gauss points for a cubic polynomial, at each of the six of which equation (1) is satisfied. In this manner the constraint is imposed both in a collocation sense and in an integral sense. Equation (7) is, nonetheless, weaker than equation (1) but not as weak as equation (6). Precise satisfaction of equation (6), and thus equation (5), will occur only for constant pressure, or in the limit as the size of the element tends to zero. Such a relaxation is also employed in the cited examples.[6–8]

The element configuration is that shown in Figure 1. However, clearly there is more to this element than is discussed here. Complete details of its construction will be presented in a future article.[11]

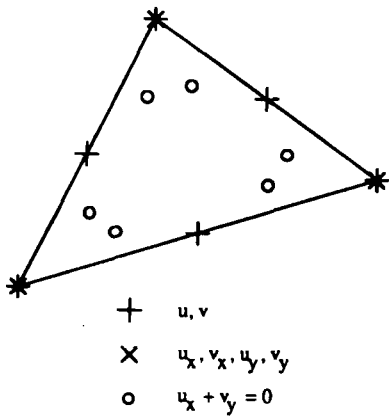


Figure 1. Solenoidal element for velocity components

## VELOCITY COMPONENTS SOLUTION

Let **u** and **v** denote the nodal parameters. Owing to the imposition of the solenoidal constraint, the local behaviour within each element is cross-coupled and therefore of the form

$$\begin{bmatrix} u \\ v \end{bmatrix} = \begin{bmatrix} \mathbf{N}^{uu} & \mathbf{N}^{uv} \\ \mathbf{N}^{vu} & \mathbf{N}^{vv} \end{bmatrix} \begin{bmatrix} \mathbf{Se} & \mathbf{0} \\ \mathbf{0} & \mathbf{Se} \end{bmatrix} \begin{bmatrix} \mathbf{u} \\ \mathbf{v} \end{bmatrix}, \tag{8}$$

where $\mathbf{N}^{uu}$, $\mathbf{N}^{uv}$, $\mathbf{N}^{vu}$ and $\mathbf{N}^{vv}$ are the interpolation functions and **Se** is the assembly operator. Substitution into the integral formulation (5) leads to the relationship

$$\begin{bmatrix} \mathbf{K}^{uu} & \mathbf{K}^{uv} \\ \mathbf{K}^{vu} & \mathbf{K}^{vv} \end{bmatrix} \begin{bmatrix} \mathbf{u} \\ \mathbf{v} \end{bmatrix} = \begin{bmatrix} \mathbf{f}^{u} \\ \mathbf{f}^{v} \end{bmatrix}, \tag{9}$$

where $\mathbf{K}^{uu}$, $\mathbf{K}^{uv}$, $\mathbf{K}^{vu}$ and $\mathbf{K}^{vv}$ are the coefficient matrices and $\mathbf{f}^{u}$ and $\mathbf{f}^{v}$ are the constant vectors. If the inertia terms are linearized by a complete first-order expansion, then

$$\begin{aligned} \mathbf{K}^{ij} = {} & \frac{1}{Re} \sum_e \mathbf{Se}^{\mathrm{T}} \int_{A_e} (\mathbf{N}_x^{vi\mathrm{T}} \mathbf{N}_x^{uj} + \mathbf{N}_x^{vi\mathrm{T}} \mathbf{N}_x^{vj} + \mathbf{N}_y^{ui\mathrm{T}} \mathbf{N}_y^{uj} + \mathbf{N}_y^{vi\mathrm{T}} \mathbf{N}_y^{vj}) \, \mathrm{d}A \, \mathbf{Se} \\ & + \sum_e \mathbf{Se}^{\mathrm{T}} \int_{A_e} \mathbf{N}^{ui\mathrm{T}} (u^* \mathbf{N}_x^{uj} + u_x^* \mathbf{N}^{uj} + v^* \mathbf{N}_y^{uj} + u_y^* \mathbf{N}^{vj}) \, \mathrm{d}A \, \mathbf{Se} \\ & + \sum_e \mathbf{Se}^{\mathrm{T}} \int_{A_e} \mathbf{N}^{vi\mathrm{T}} (u^* \mathbf{N}_x^{vj} + v_x^* \mathbf{N}^{uj} + v^* \mathbf{N}_y^{vj} + v_y^* \mathbf{N}^{vj}) \, \mathrm{d}A \, \mathbf{Se} \end{aligned} \tag{10a}$$

$$\begin{aligned} \mathbf{f}^{i} = {} & \sum_e \mathbf{Se}^{\mathrm{T}} \int_{A_e} [\mathbf{N}^{ui\mathrm{T}} (u^* u_x^* + v^* u_y^*) + \mathbf{N}^{vi\mathrm{T}} (u^* v_x^* + v^* v_y^*)] \, \mathrm{d}A \\ & + \sum_e \mathbf{Se}^{\mathrm{T}} \int_{S_e} \left[ \mathbf{N}^{ui\mathrm{T}} \left( \frac{1}{Re} u_n - \alpha p \right) + \mathbf{N}^{vi\mathrm{T}} \left( \frac{1}{Re} v_n - \beta p \right) \right] \mathrm{d}s. \end{aligned} \tag{10b}$$

Here an asterisk denotes the value from the previous iteration of the variable or its derivatives. The complete specification of the solution therefore requires

$$u \quad \text{or} \quad \frac{1}{Re} u_n - \alpha p, \qquad \frac{1}{Re} v_n - \beta p$$

and

$$v \quad \text{or} \quad \frac{1}{Re} u_n - \alpha p, \qquad \frac{1}{Re} v_n - \beta p$$

to be supplied as boundary conditions. In this manner equation (9) permits the velocity components to be determined solely from their own values at the previous iteration.

## PRESSURE SOLUTION

Once the velocity components are known, an obvious course for the retrieval of the pressure is to combine the original governing equations to form

$$\nabla^2 p = -(u_x^2 + 2v_x u_y + v_y^2). \tag{11}$$

Application of the Bubnov–Galerkin method then requires either the pressure or its normal gradient to be specified around the entire boundary.

In most cases knowledge of the pressure is restricted to a lone datum value. On the rest of the boundary the normal gradient must come from equation (2). Now a valid pressure solution must have

$$-\int_A (u_x^2 + 2v_x u_y + v_y^2)\,\mathrm{d}A = \int_s \left[\alpha\left(\frac{1}{Re}\nabla^2 u - uu_x - vu_y\right) + \beta\left(\frac{1}{Re}\nabla^2 v - uv_x - vv_y\right)\right]\mathrm{d}s, \quad (12)$$

by reason of Gauss's theorem, and so a Poisson equation procedure is not viable owing to the inability to obtain accurate estimates of all these terms, especially the highest-order derivatives and products of derivatives. Even smoothing of the numerical noise is not sufficiently effective. As a consequence, some alternative procedure is needed which reduces the highest-order derivatives and stipulates the 'natural' boundary conditions.

A novel idea for the retrieval of the pressure which meets both these requirements starts with the boundary value problem posed, not by the entire domain, but by each element on its own. Furthermore, to avoid the need to patch neighbouring solutions, the solution is found in terms of the auxiliary pressure gradients $Px$ and $Py$ rather than the pressure itself. Employment of the Petrov–Galerkin method, where the weighting function $\mathbf{W}$ is not solenoidal, gives

$$\int_{A_e} \mathbf{W}^{\mathrm{T}}\left(\frac{1}{Re}\nabla^2 u - Px - uu_x - vu_y\right)\mathrm{d}A = \mathbf{0}, \quad (13a)$$

$$\int_{A_e} \mathbf{W}^{\mathrm{T}}\left(\frac{1}{Re}\nabla^2 v - Py - uv_x - vv_y\right)\mathrm{d}A = \mathbf{0}, \quad (13b)$$

whereupon the utilization of Green's theorem yields

$$\frac{1}{Re}\int_{A_e} (\mathbf{W}_x^{\mathrm{T}} u_x + \mathbf{W}_y^{\mathrm{T}} u_y)\,\mathrm{d}A + \int_{A_e} \mathbf{W}^{\mathrm{T}}(Px + uu_x + vu_y)\,\mathrm{d}A = \mathbf{0}, \quad (14a)$$

$$\frac{1}{Re}\int_{A_e} (\mathbf{W}_x^{\mathrm{T}} v_x + \mathbf{W}_y^{\mathrm{T}} v_y)\,\mathrm{d}A + \int_{A_e} \mathbf{W}^{\mathrm{T}}(Py + uv_x + vv_y)\,\mathrm{d}A = \mathbf{0}, \quad (14b)$$

if the weighting function can be made to vanish on the boundary of the element. This important operation therefore reduces the highest-order derivatives without the extra contribution of a boundary integral.

Suppose the local behaviour in terms of the nodal parameters $\mathbf{Px}$ and $\mathbf{Py}$ is expressible as

$$\begin{bmatrix} Px \\ Py \end{bmatrix} = \begin{bmatrix} \mathbf{N} & \mathbf{0} \\ \mathbf{0} & \mathbf{N} \end{bmatrix}\begin{bmatrix} \mathbf{Px} \\ \mathbf{Py} \end{bmatrix}, \quad (15)$$

where $\mathbf{N}$ is the interpolation function. The auxiliary pressure gradients are obtainable from

$$\begin{bmatrix} \mathbf{K} & \mathbf{0} \\ \mathbf{0} & \mathbf{K} \end{bmatrix}\begin{bmatrix} \mathbf{Px} \\ \mathbf{Py} \end{bmatrix} = \begin{bmatrix} \mathbf{f}^{Px} \\ \mathbf{f}^{Py} \end{bmatrix}, \quad (16)$$

where

$$\mathbf{K} = \int_{A_e} \mathbf{W}^{\mathrm{T}}\mathbf{N}\,\mathrm{d}A, \tag{17a}$$

$$\begin{aligned}\mathbf{f}^{\mathrm{Px}} &= -\frac{1}{Re}\int_{A_e}(\mathbf{W}_x^{\mathrm{T}}u_x + \mathbf{W}_y^{\mathrm{T}}u_y)\,\mathrm{d}A - \int_{A_e}\mathbf{W}^{\mathrm{T}}(uu_x + vu_y)\,\mathrm{d}A,\\ \mathbf{f}^{\mathrm{Py}} &= -\frac{1}{Re}\int_{A_e}(\mathbf{W}_x^{\mathrm{T}}v_x + \mathbf{W}_y^{\mathrm{T}}v_y)\,\mathrm{d}A - \int_{A_e}\mathbf{W}^{\mathrm{T}}(uv_x + vv_y)\,\mathrm{d}A,\end{aligned} \tag{17b}$$

provided $\mathbf{K}$ is square.

The solenoidal element now serves a further purpose, not to eliminate the pressure, but to retrieve it. To be specific, its nodal parameters act as boundary conditions. Suppose $\mathbf{W}$ derives from a quartic polynomial defined by 15 nodal parameters. Known boundary values make all except three redundant. Therefore, if $\mathbf{N}$ derives from a linear polynomial, equation (16) is rendered solvable. The resulting system comprises two sets of three equations in three unknowns.

With the pressure gradients now known over each element, the pressure over the entire domain can be determined from a least squares fit. In terms of the nodal parameter $\mathbf{p}$, let the local behaviour within each element be representable as

$$p = \mathbf{N}^{\mathrm{p}}\mathbf{Se}^{\mathrm{p}}\mathbf{p}, \tag{18}$$

where $\mathbf{N}^{\mathrm{p}}$ is the interpolation function and $\mathbf{Se}^{\mathrm{p}}$ is the assembly operator. A continuous pressure over the domain is produced upon minimization of the least squares functional

$$I = \tfrac{1}{2}\int_A [(p_x - Px)^2 + (p_y - Py)^2]\,\mathrm{d}A. \tag{19}$$

With respect to each nodal parameter, this occurs when

$$\frac{1}{2}\frac{\partial}{\partial \mathbf{p}}\sum_e \int_{A_e} [(\mathbf{N}_x^{\mathrm{p}}\mathbf{Se}^{\mathrm{p}}\mathbf{p} - Px)^2 + (\mathbf{N}_y^{\mathrm{p}}\mathbf{Se}^{\mathrm{p}}\mathbf{p} - Py)^2]\,\mathrm{d}A = \mathbf{0}. \tag{20}$$

Thus

$$\mathbf{K}^{\mathrm{p}}\mathbf{p} = \mathbf{f}^{\mathrm{p}}, \tag{21}$$

in which

$$\mathbf{K}^{\mathrm{p}} = \sum_e \mathbf{Se}^{\mathrm{p}^{\mathrm{T}}}\int_{A_e}(\mathbf{N}_x^{\mathrm{p}^{\mathrm{T}}}\mathbf{N}_x^{\mathrm{p}} + \mathbf{N}_y^{\mathrm{p}^{\mathrm{T}}}\mathbf{N}_y^{\mathrm{p}})\,\mathrm{d}A\;\mathbf{Se}^{\mathrm{p}}, \tag{22a}$$

$$\mathbf{f}^{\mathrm{p}} = \sum_e \mathbf{Se}^{\mathrm{p}^{\mathrm{T}}}\int_{A_e}(\mathbf{N}_x^{\mathrm{p}^{\mathrm{T}}}Px + \mathbf{N}_y^{\mathrm{p}^{\mathrm{T}}}Py)\,\mathrm{d}A \tag{22b}$$

demonstrate that there is no requirement for boundary conditions other than a lone datum value, which is consistent with the physics.

So as not to waste valuable information, if the gradients vary linearly, then it is sensible to have the pressure vary quadratically. The resulting Lagrange pressure element therefore shares identical nodes with its solenoidal counterpart, as illustrated in Figure 2.

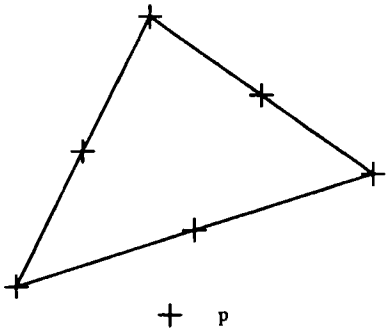


Figure 2. Element for pressure

## SOLFEM CODE

The described solution procedures form the basis of the SOLFEM code which, together with the velocity components and the pressure, provides solutions for the streamfunction, the vorticity, the shear stress and the velocity divergence. The code consists of a sequence of separate programmes which capitalizes on the independence of the solution variables to minimize storage requirements. A further advantage of this structure is that critical values are known in advance, so that exact array dimensions can be set before the execution of each programme. Solution is by means of a frontal scheme. The entire code is written from scratch, even to the extent of the graphics.

The solenoidal element reduces the storage requirements, not only through the decoupling of the solution, but also owing to its first-derivative nodal parameters. For the 8800-element backward step problem which follows, the savings over a Lagrange element are these. At the expense of the increase in the number of degrees of freedom at the vertex nodes, the total number of nodes themselves is reduced from 44,721 to 17,961. The number of degrees of freedom which are active is reduced from 86,681 to 52,106. An indication of the efficiency of the code is a storage requirement from variable declarations of 1·77 Mbytes, even with double precision, for this problem.

## NUMERICAL EXPERIMENTS

The validity of the ideas which are discussed in this paper and implemented in the SOLFEM code is tested by the application of the code to some classical benchmark problems. Convergence is considered to occur when the maximum change in nodal values of velocity components between successive iterations is less than $10^{-5}$.

Where possible, the results are compared with those from the literature and the commercial codes, FLUENT and FIDAP. The former is a finite volume code. The latter is a finite element code, either with a penalty function formulation or with a Lagrange multiplier formulation, the results from which are almost identical. At this early stage in the comparison exercise, for each code, a mesh which is at most slightly graded and certainly not optimum is employed. Therefore, any discrepancy between the results of the codes is more likely to be related to a deficiency in the resolution of the meshes than to a deficiency in the capabilities of the codes themselves.

*Square cavity*

The flow in a square cavity, maintained by the driving action of a sliding lid, is a prototype for flows with recirculation. The problem is recognized as a standard test case and as a consequence possesses a rich literature, a relevant sample of which is References 12–14. When comparing results, however, care has to be exercised owing to the different treatments of the singularities at the corners near the lid. For the present case, the corners are considered to be part of the walls, not the lid, to prevent flow through the walls.

Generally, the principal feature of the flow is a primary vortex. As well, there are secondary vortices of much lesser strength which rotate in the reverse sense. At low Reynolds numbers the core of the primary vortex is located about a quarter of the depth from the lid and equidistant from the walls. A pair of secondary vortices is located in the corners opposite the lid. With increasing Reynolds numbers the core of the primary vortex moves in the flow direction then towards the cavity centre. Both of the secondary vortices grow in size, although not at the same rate. At high Reynolds numbers the cavity reduces, in essence, to an inviscid recirculating eddy surrounded by a viscous boundary layer. A further secondary vortex appears on the wall near the start of the lid.

Included here are results for various mesh densities and various Reynolds numbers. Meshes are

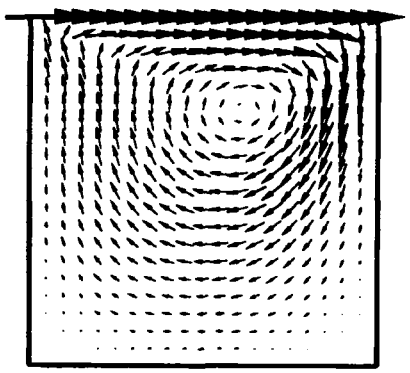

Figure 3. Velocity vectors for square cavity, $Re = 100$

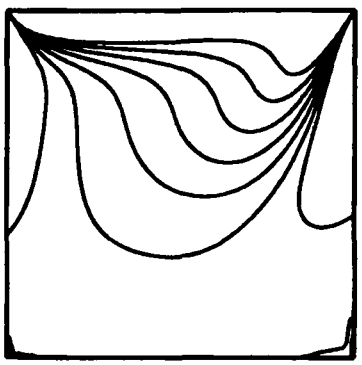

Figure 4. Vorticity contours for square cavity, $Re = 100$ ($\omega = -5, -4, -3, -2, -1, 0, 1$)

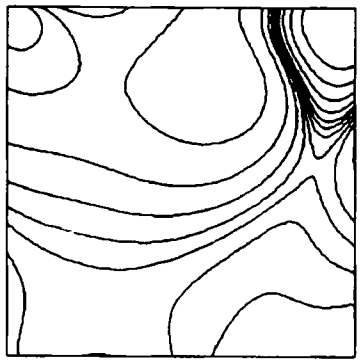

FLUENT

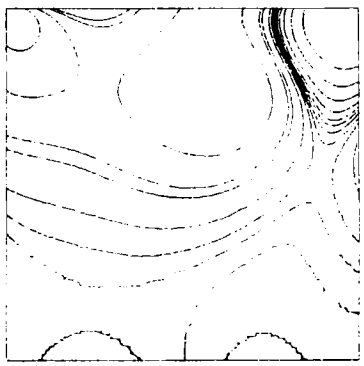

FIDAP

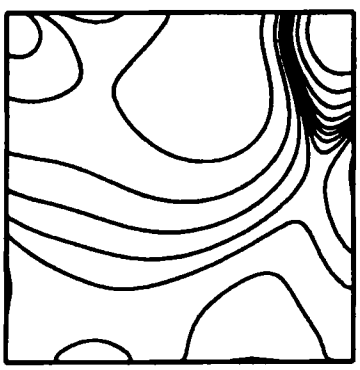

SOLFEM

Figure 5. Pressure contours for square cavity, $Re = 100$ ($p = -0{\cdot}12, -0{\cdot}06, -0{\cdot}03, -0{\cdot}015, -0{\cdot}0075, -0{\cdot}00375, 0, 0{\cdot}00375, 0{\cdot}0075, 0{\cdot}015, 0{\cdot}03, 0{\cdot}06, 0{\cdot}12$)

composed of almost uniform triangle pairs, with the mesh density $m$ denoted by the number of these pairs along each side. Solutions for the velocity components at any Reynolds number are initiated from the solution at the previous Reynolds number. Convergence never takes more than five iterations. Sample solutions for $m = 41$ and $Re = 100$ are presented in Figures 3–9. These encompass velocity vectors, vorticity contours, pressure contours, streamfunction contours, wall pressure coefficient profiles, skin friction coefficient profiles and centreline velocity

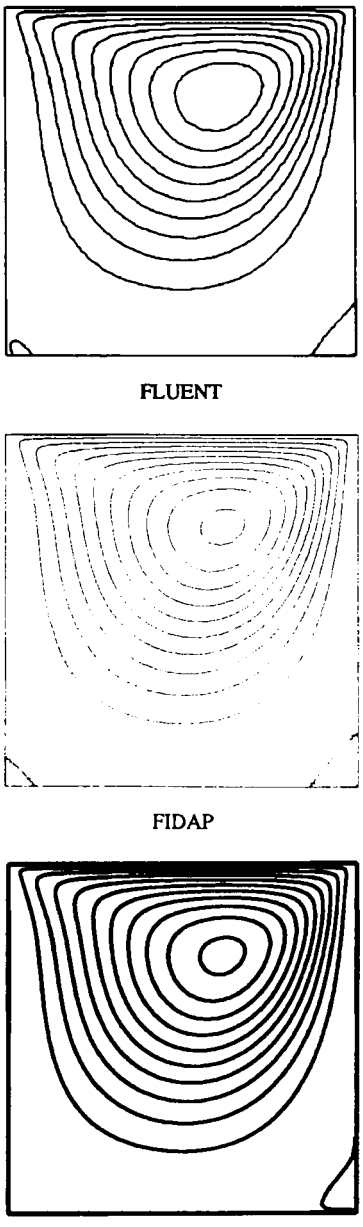


Figure 6. Streamfunction contours for square cavity, $Re = 100$ ($\psi = -0{\cdot}1, -0{\cdot}09, -0{\cdot}08, -0{\cdot}07, -0{\cdot}06, -0{\cdot}05, -0{\cdot}04, -0{\cdot}03, -0{\cdot}02, -0{\cdot}01, 0$)

profiles. Figure 10 shows the movement of the vortex core with increasing Reynolds number for $m = 41$, as does Table I. Table II details the characteristics of the vortex core with increasing mesh density for $Re = 100$. In all cases the solutions are in agreement with published results.[12–14] Moreover, good agreement is obtained with the results from the commercial codes. These employ slightly graded meshes, FLUENT using $66 \times 66$ cells and FIDAP using

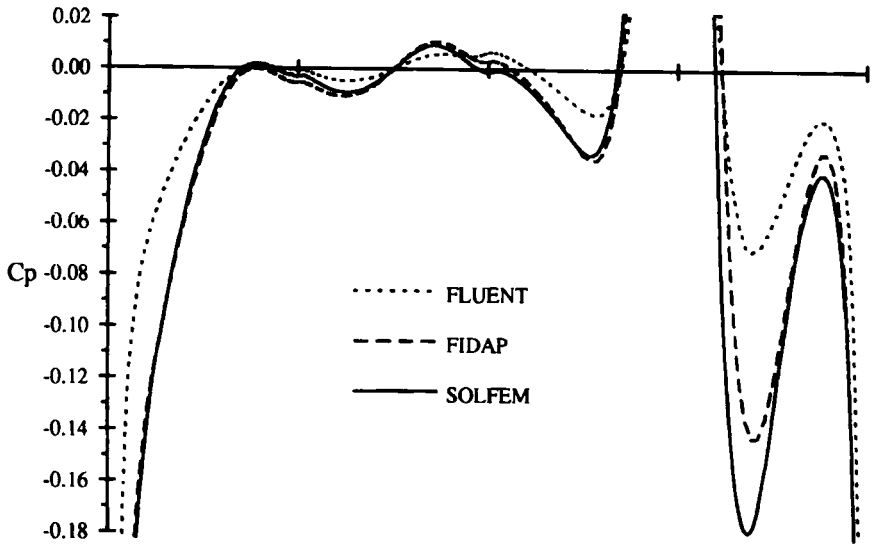


Figure 7. Wall pressure coefficient profiles for square cavity, $Re = 100$ (on horizontal axis, tick marks denote cavity corners, last division represents sliding lid)

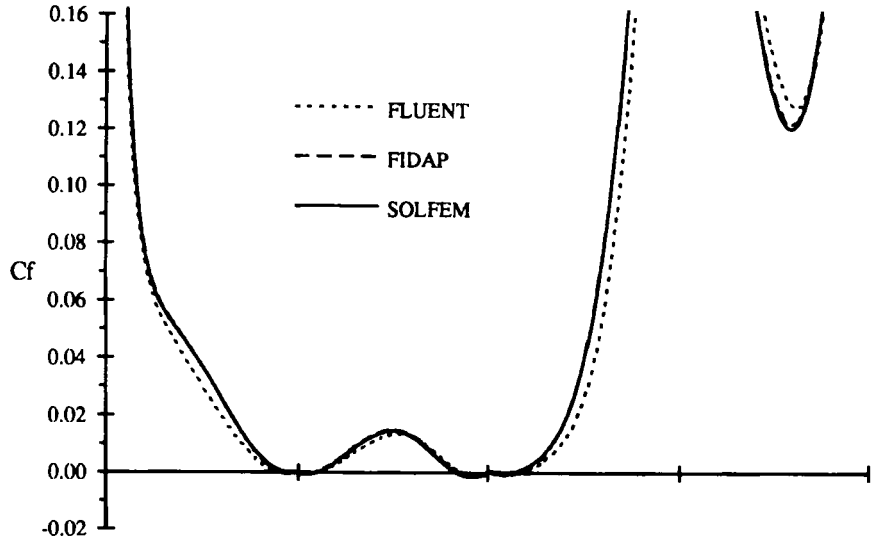


Figure 8. Skin friction coefficient profiles for square cavity, $Re = 100$ (on horizontal axis, tick marks denote cavity corners, last division represents sliding lid)

80 × 80 elements. Where agreement is not so good appears to be caused by different estimates of velocity gradients, mainly due to different-order interpolations which are not compensated for by the meshes in the region between the singularities. Finally, the improvement in the solution with the refinement of the mesh can be clearly seen from Table II. Whether this convergence is to the true solution awaits further tests, since there is still some disagreement

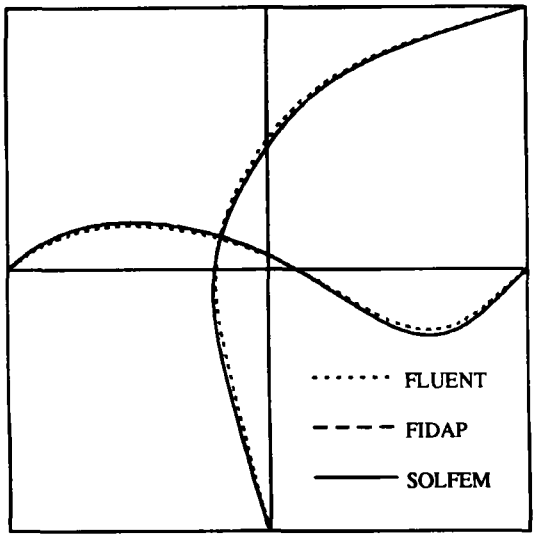


Figure 9. Centreline velocity profiles for square cavity, $Re = 100$

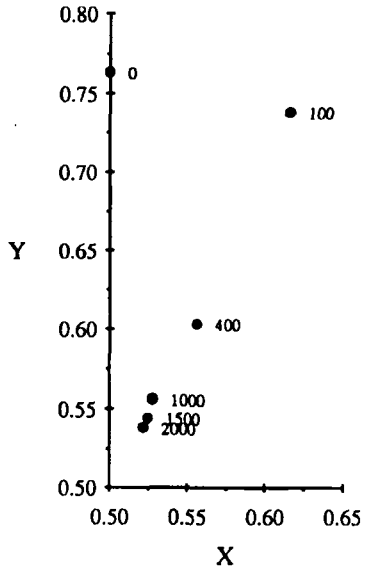


Figure 10. Location of vortex core for square cavity, $m = 41$

between the results in the literature, more so with the properties at the vortex core than its actual location.

*Backward step*

Another established benchmark problem involves vortex formation, this time caused by a sudden change in the test section. This problem is the flow through a channel over a single

Table I. Location of vortex core for square cavity, $m = 41$

| | | Vortex core | |
|---|---|---|---|
| *Re* | Code | *x* | *y* |
| 0 | FLUENT | 0·500 | 0·765 |
| | FIDAP | 0·500 | 0·766 |
| | SOLFEM | 0·500 | 0·763 |
| | Reference 13 | 0·50 | 0·76 |
| 100 | FLUENT | 0·620 | 0·748 |
| | FIDAP | 0·618 | 0·731 |
| | SOLFEM | 0·616 | 0·738 |
| | Reference 14 | 0·617 | 0·734 |
| | Reference 13 | 0·62 | 0·74 |
| 400 | FLUENT | 0·565 | 0·601 |
| | FIDAP | 0·563 | 0·618 |
| | SOLFEM | 0·556 | 0·603 |
| | Reference 14 | 0·555 | 0·606 |
| | Reference 13 | 0·55 | 0·60 |
| 1000 | FLUENT | 0·565 | 0·557 |
| | FIDAP | 0·531 | 0·561 |
| | SOLFEM | 0·528 | 0·556 |
| | Reference 14 | 0·531 | 0·563 |
| | Reference 13 | 0·53 | 0·56 |
| 1500 | FLUENT | 0·557 | 0·557 |
| | FIDAP | 0·529 | 0·559 |
| | SOLFEM | 0·525 | 0·544 |
| | Reference 13 | 0·53 | 0·55 |
| 2000 | FLUENT | 0·543 | 0·543 |
| | FIDAP | 0·521 | 0·543 |
| | SOLFEM | 0·522 | 0·538 |
| | Reference 13 | 0·52 | 0·54 |

Table II. Properties at vortex core for square cavity, $Re = 100$

| | Vortex core properties | | | | |
|---|---|---|---|---|---|
| *m* | *x* | *y* | $\omega$ | *p* | $\psi$ |
| 6 | 0·625 | 0·750 | −3·31 | −0·0736 | −0·096 |
| 11 | 0·613 | 0·738 | −3·01 | −0·0877 | −0·101 |
| 16 | 0·617 | 0·742 | −3·12 | −0·0927 | −0·102 |
| 21 | 0·619 | 0·738 | −3·13 | −0·0941 | −0·102 |
| 31 | 0·617 | 0·738 | −3·12 | −0·0958 | −0·102 |
| 41 | 0·616 | 0·738 | −3·11 | −0·0966 | −0·103 |
| Reference 14 | 0·617 | 0·734 | −3·17 | — | −0·103 |
| Reference 13 | 0·62 | 0·74 | −3·10 | −0·0953 | −0·104 |

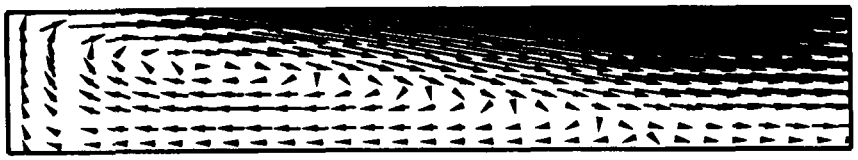

Figure 11. Velocity vectors up to six step heights behind backward step, $Re = 100$

backward-facing step. The flow is characterized by separation near the upstream corner and reattachment on the downstream wall. This results in the formation of a vortex behind the face of the step. Of principal interest is the reattachment length, together with the vortex strength. With an increase in the Reynolds number, a smaller vortex of lesser strength forms downstream on the opposite wall.

This problem has been the subject of considerable investigation, both experimental, to gain an understanding of the underlying physics, and computational, to test the efficacy of a mathematical model. Listed in the references are several of the more extensive investigations.[15–17] Unfortunately, the usefulness of the problem as a source of comparable data is hampered by the lack of a standard for its specification. This concerns the domain geometry and the boundary conditions, but extends even to the definition of the Reynolds number.

For the present case, the expansion ratio is 2:3, while the channel is two step heights long before the step and 28 step heights long after the step. The solid walls exhibit no slip, the inlet has a parabolic velocity profile and the outlet has zero normal velocity gradients. An almost uniform mesh of 8800 elements is employed. Note that a count of triangular elements can appear inflated, since the elements tend to exist in pairs. The Reynolds number is based on the step height and the maximum velocity. Solutions for $Re = 100$ are provided in Figures 11–15. These comprise velocity vectors, vorticity contours, streamfunction contours, skin friction coefficient profiles and streamwise velocity profiles. Again, the solutions generally agree with those from the commercial codes. FLUENT uses 4192 graded cells. FIDAP uses 3920 graded elements. The agreement with physical experiments is not so close, owing in part to the variance in their results.[18]

While the reattachment point is apparent from Figure 13, a precise estimate of its location from this figure is hindered by the fact that each code determines the streamfunction as a derived quantity, with a resulting increase in opportunity for error. In the region near the dividing streamline, especially near the reattachment point, gradients are small and so a small error in the streamfunction produces a large movement of the streamline. This characteristic is not unique, either to the present work or to the present problem. Obtaining an accurate depiction of the dividing streamline is a common concern. Another estimate of the location of the

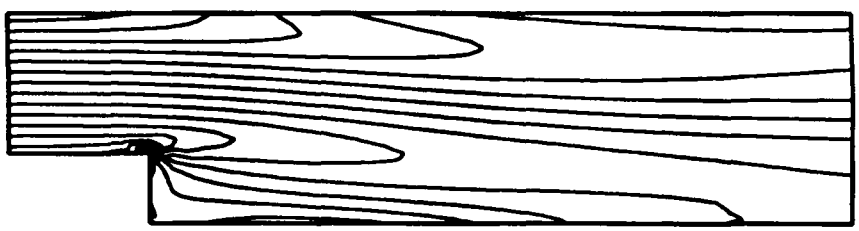

Figure 12. Vorticity contours up to 10 step heights behind backward step, $Re = 100$ ($\omega = -2{\cdot}4, -2{\cdot}1, -1{\cdot}8, -1{\cdot}5, -1{\cdot}2, -0{\cdot}9, -0{\cdot}6, -0{\cdot}3, 0, 0{\cdot}3, 0{\cdot}6, 0{\cdot}9, 1{\cdot}2, 1{\cdot}5, 1{\cdot}8$)

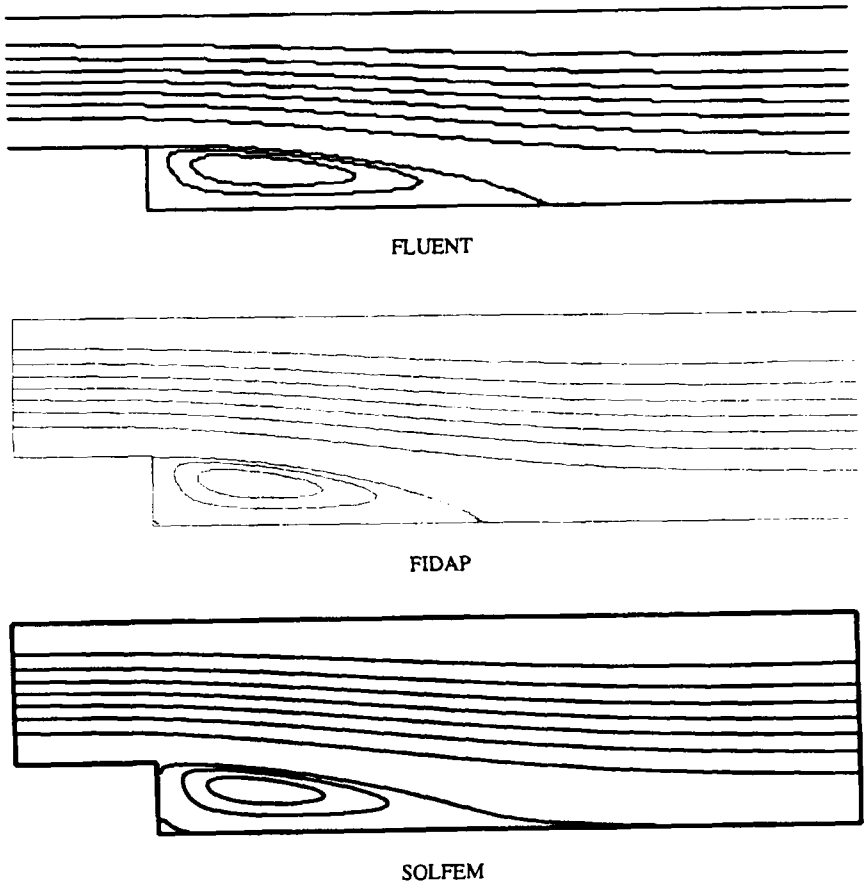


Figure 13. Streamfunction contours up to 10 step heights behind backward step, $Re = 100$ ($\psi = -0{\cdot}02, -0{\cdot}01, 0, 0{\cdot}167, 0{\cdot}333, 0{\cdot}5, 0{\cdot}667, 0{\cdot}833, 1, 1{\cdot}167, 1{\cdot}333$)

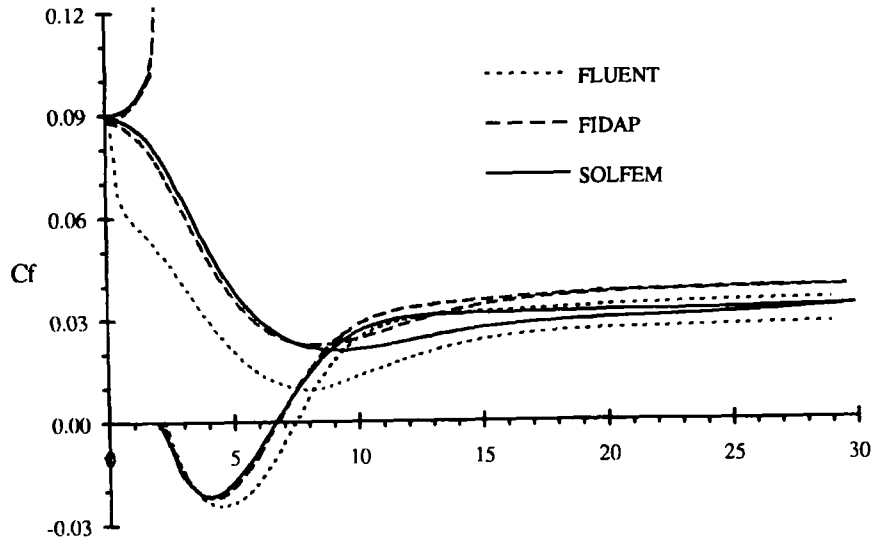


Figure 14. Skin friction coefficient profiles for backward step, $Re = 100$ (discontinuous curves pertain to stepped wall)

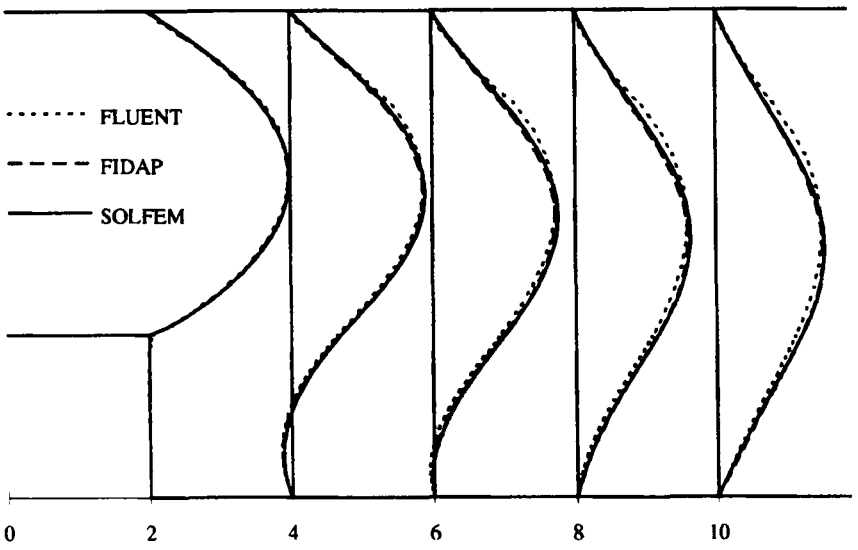


Figure 15. Streamwise velocity profiles up to eight step heights behind backward step, $Re = 100$

reattachment point can be obtained from Figure 15. However, a far better estimate can be obtained from Figure 14. Here the discontinuous curves represent the profiles along the wall with the step. The discontinuity is caused by the omission of the profile over the face of the step, owing to the conflict in the plot scales. The reattachment point occurs at the point of change of the sign of the skin friction coefficient.

## CONCLUSIONS

A comparison of the SOLFEM results with those from other sources shows good agreement in most cases. At times it is even almost impossible to differentiate between results. Where the agreement is most pleasing is in the severe tests posed by the comparisons of the profiles, along with all plots of the derived quantities, especially the pressure, which is known for its sensitivity to any noise in the prime solution.

At this point it is important to realize that the purpose of this whole exercise was to validate the SOLFEM code, not to conduct a definitive comparison of the performance of the various codes. For a start, the circumstances under which the exercise was conducted do not allow such a comparison. The different codes were run on different platforms, each with different resources. The meshes were not optimum ones. Any attempt, therefore, to make claims of superiority of one code over the others, based on these results alone, would be invalid. The exercise, however, is in its early stages and further work, in particular with graded meshes of similar resolution for all codes, is planned for the future. Higher Reynolds numbers are also proposed.

As well as different platforms, there is the matter of different philosophies. The SOLFEM code is designed to minimize storage requirements, on the basis that a fast code is of little benefit if it cannot fit on the available platform. It could alternatively be designed to minimize processor time. Such a change in philosophy, and the subsequent change in performance, would have no connection with the inherent features of the solenoidal approach. Whatever their design

philosophies, similar statements are applicable to the other codes. Thus, given such diverse conditions, any attempt to compare the performance of the various codes with measures, either of storage requirements or of processor time, would be inappropriate.

What can be claimed here, however, is that, given equivalent conditions, the SOLFEM code would be at least competitive with the others. Thus, what then are the main features of the solenoidal approach and in particular of the solenoidal element?

The solenoidal approach decouples the solution so that the velocity components are determined solely from their own values at the previous iteration. Once the velocity components have been determined, the pressure can be retrieved when desired, like any other derived quantity. The advantage of this approach is that there is a reduction in the dimensions of the problem, with a consequent reduction in the storage requirements.

The solenoidal element is conforming. It possesses first-derivative nodal parameters and this again reduces the problem dimensions. Owing to the imposition of an external constraint, it has cross-coupled local behaviour, which appears unique. Since a pointwise solenoidal element which is conforming is not possible, the constraint is relaxed to produce an elementwise solenoidal element. This means that the approach is exact only for constant pressure. Otherwise it becomes exact as the size of the element tends to zero, like any other valid approach. What is more, the same element which is responsible for the elimination of the pressure also plays a role in its eventual retrieval.

In what are significant tests, the benchmark applications demonstrate the worth of the approach and of the element in particular. However, their use is applicable, not just to these test cases, but to any flow problem whose behaviour is governed by the stated differential equations. The sole requirement, as always, is that the domain be such as to permit the specification of the stated boundary conditions.

The question that remains is the one about possible extensions beyond current applications. In theory, an extension in the spatial dimensions is possible, through the use of elements in the shape of triangular pyramids. The trick, once again, is to determine the appropriate polynomial. Apart from an increase in the complexity of the code, such an extension is achievable at no further cost than for any other approach. An extension to the temporal dimension is also possible. In fact, this has been achieved[4] through the use of elements in the shape of triangular prisms. High-order time discretizations can be achieved by the overlapping of the time intervals. Excellent results have been obtained in limited trials against more standard time-stepping schemes. Finally, this whole concept is not restricted to viscous flows, but is applicable wherever there is a similar pairing in the governing equations of a pressure-like term with a velocity-like divergence term.

ACKNOWLEDGEMENT

The author wishes to thank B. R. Pearson for the generation of the results from the commercial codes. FLUENT is a product of Creare Inc., Hanover, NH, U.S.A. FIDAP is a product of Fluid Dynamics International Inc., Evanston, IL, U.S.A.

## APPENDIX: NOMENCLATURE

| | |
|---|---|
| $A$ | solution domain |
| $\mathbf{f}^p$ | constant vector for pressure |
| $\mathbf{f}^{p_x}$, $\mathbf{f}^{p_y}$ | constant vectors for auxiliary pressure gradients |

| | |
|---|---|
| $\mathbf{f}^u$, $\mathbf{f}^v$ | constant vectors for velocity components |
| $I$ | least squares functional |
| $\mathbf{K}$ | coefficient matrix for auxiliary pressure gradients |
| $\mathbf{K}^p$ | coefficient matrix for pressure |
| $\mathbf{K}^{uu}$, $\mathbf{K}^{uv}$, $\mathbf{K}^{vu}$, $\mathbf{K}^{vv}$ | coefficient matrices for velocity components |
| $m$ | mesh density |
| $n$ | outward normal |
| $\mathbf{N}$ | interpolation function for auxiliary pressure gradients |
| $\mathbf{N}^p$ | interpolation function for pressure |
| $\mathbf{N}^{uu}$, $\mathbf{N}^{uv}$, $\mathbf{N}^{vu}$, $\mathbf{N}^{vv}$ | interpolation functions for velocity components |
| $p$ | pressure |
| $\mathbf{p}$ | nodal parameter for pressure |
| $Px$, $Py$ | auxiliary pressure gradients |
| $\mathbf{Px}$, $\mathbf{Py}$ | nodal parameters for auxiliary pressure gradients |
| $Re$ | Reynolds number |
| $s$ | domain boundary |
| $\mathbf{Se}$ | assembly operator for velocity components |
| $\mathbf{Se}^p$ | assembly operator for pressure |
| $u$, $v$ | velocity components |
| $\mathbf{u}$, $\mathbf{v}$ | nodal parameters for velocity components |
| $\mathbf{W}$ | weighting function |
| $x$, $y$ | Cartesian co-ordinates |

*Greek letters*

| | |
|---|---|
| $\alpha$, $\beta$ | direction cosines for outward normal |
| $\psi$ | streamfunction |
| $\omega$ | vorticity |

## REFERENCES


1. S. Tuann and M. Olson, 'Review of computing methods for recirculating flows', *J. Comput. Phys.*, **29**, 1–19 (1978).
2. D. Norrie and G. de Vries, 'A survey of the finite element applications in fluid mechanics', in R. Gallagher, O. Zienkiewicz, J. Oden, M. Cecchi and C. Taylor (eds), *Finite Elements in Fluids*, Vol. 3, Wiley, Chichester, 1978.
3. A. N. F. Mack, 'An uncoupled approach for primitive variable solutions to viscous incompressible flows', *Proc. 3rd Int. Conf. on Finite Elements in Flow Problems*, Banff, 1980, Vol. 1, pp. 121–131.
4. A. N. F. Mack, 'A solenoidal approach to viscous flow simulation,' *PhD Thesis*, University of Sydney, 1983.
5. A. N. F. Mack, 'A unification of finite element approaches for primitive variable solutions to viscous incompressible flows', in J. Noye and C. Fletcher (eds), *Computational Techniques and Applications*, North-Holland, Amsterdam, 1984.
6. M. Fortin, 'Approximation des fonctions a divergence nulle par la methode des elements finis', *Proc. 3rd Int. Conf. on Numerical Methods in Fluid Mechanics*, Paris, 1972, pp. 99–103.
7. D. F. Griffiths, 'The construction of approximately divergence-free finite elements', *Proc. 3rd Conf. on the Mathematics of Finite Elements and Applications*, Uxbridge, 1978, pp. 237–245.
8. R. Temam, 'Some finite element methods in fluid flow', *Proc. 6th Int. Conf. on Numerical Methods in Fluid Dynamics*, Tbilisi, 1978, pp. 34–55.
9. X. Ye and C. Hall, 'The construction of an optimal weakly divergence-free macroelement', *Int. j. numer. methods eng.*, **36**, 2245–2262 (1993).
10. A. N. F. Mack, 'A solenoidal element for inherent mass conservation', in W. L. Hogarth and B. J. Noye (eds), *Computational Techniques and Applications*, Hemisphere, New York, 1990.
11. A. N. F. Mack, 'The construction of an element level zero-divergence finite element', in preparation.
12. O. R. Burggraf, 'Analytical and numerical studies of the structure of steady separated flows', *J. Fluid Mech.*, **24**, 113–151 (1966).

13. M. Olson and S. Tuann, 'New finite element results for the square cavity', *Comput. Fluids*, **7**, 123–135 (1979).
14. U. Ghia, K. Ghia and C. Shin, 'High-*Re* solutions for incompressible flow using the Navier–Stokes equations and a multigrid method', *J. Comput. Phys.*, **48**, 387–411 (1982).
15. D. J. Atkins, S. J. Maskell and M. A. Patrick, 'Numerical prediction of separated flows', *Int. j. numer. methods eng.*, **15**, 129–144 (1980).
16. B. Armaly, F. Durst, J. Pereira and B. Schonung, 'Experimental and theoretical investigation of backward-facing step flow', *J. Fluid Mech.*, **127**, 473–496 (1983).
17. K. Morgan, J. Periaux and F. Thomasset (eds), *Notes on Numerical Fluid Mechanics*, Vol. 9, *Analysis of Laminar Flow over a Backward Facing Step*, Vieweg, Braunschweig, 1984.
18. W. Adams and P. Johnston, 'Effects of the separating shear layer on the reattachment flow structure', *Exp. Fluids*, **6**, 493–499 (1988).